

# Flocking with random non-reciprocal interactions

Jiwon Choi<sup>1</sup>, Jae Dong Noh<sup>2</sup>, Heiko Rieger<sup>1</sup>

<sup>1</sup> *Department of Physics & Center for Biophysics,*

*Saarland University, Campus E2 6, 66123 Saarbrücken, Germany*

<sup>2</sup> *Department of Physics, University of Seoul, Seoul, 02504, Korea*

(Dated: June 30, 2025)

Flocking is ubiquitous in nature and emerges due to short or long range alignment interactions among self-propelled agents. Two unfriendly species that anti-align or even interact non-reciprocally show more complex collective phenomena, ranging from parallel and anti-parallel flocking over run-and chase behavior to chiral phases. Whether flocking or any of these collective phenomena can survive in the presence of a large number of species with random non-reciprocal interactions remained elusive so far. As a first step here the extreme case of a Vicsek-like model with fully random non-reciprocal interactions between the individual particles is considered. As soon as the alignment bias is of the same order as the random interactions the ordered flocking phase occurs, but deep within this phase, the random non-reciprocal interactions can still support global chiral and oscillating states in which the collective movement direction rotates or oscillates slowly. For short-range interactions, moreover, even without alignment bias self-organized cliques emerge, in which medium size clusters of particles that have predominantly aligning interactions meet accidentally and stay together for macroscopic times. These results may serve as a starting point for the study of multi-species flocking models with non-random but complex non-reciprocal inter-species interactions.

*Introduction:* – Active matter consists of particles that consume energy to use it as a fuel for movement, force generation, deformation or proliferation [1–4] and gives rise to collective phenomena that are absent in equilibrium systems, like flocking [5], motility induced phase separation [6], spontaneously flowing matter [7, 8] or living crystals [9, 10]. Recently active matter with non-reciprocal interactions (NRI) has attracted a lot of attention, for which paradigmatic examples are the predator-prey relationship, visual perception [11, 12] or flocking of unfriendly species [13–17]. The hallmark of NRI is the emergence of a broad range of fascinating phenomena ranging from the spontaneous emergence of travelling waves [18, 19] and chiral states [13] to odd viscosity [20], elasticity [21] and diffusivity [22, 23].

In systems consisting of particles with only two-body interactions non-reciprocity manifests itself by the violation of Newton’s law “*actio=reactio*” such that the force or influence exerted by particle  $j$  on particle  $i$ ,  $F_{ij}$  is *not* equal to  $-F_{ji}$ . In complex systems with many species of particles NRI can be encoded in a non-symmetric interaction matrix  $J_{ij}$ , as for instance by non-symmetric reaction rates for chemical mixtures or predator-prey systems. For complex systems consisting of a large number of species this interaction matrix is frequently assumed to be random as in the context of neural networks [24–27], ecological communities [28–31], the immune system [32], coupled oscillators [33–36] and multi-species suspensions [37]. Random-field type disorder, meaning heterogeneous environments instead of interactions, has been studied for the Vicsek model [38–42] and scalar active matter [43, 44], but the impact of random non-reciprocal (NR) alignment interactions on flocking systems remains elusive.

Large ensembles of self-propelled particles may consist of many species with varying inter-species interactions,

each of which can be aligning for friendly species or anti-aligning for unfriendly species [45]. In the simplest case of only two species NRI gives rise to run-and chase states, a travelling wave in which one species follows the other, and chiral states, in which all particles perform a coherent rotation [13–15, 17], in addition to the still possible flocking state, in which all particles move collectively in the same direction. Whether these collective phenomena can survive in the presence of NRI in a multi-species system is the question that we will address in this paper. Under which circumstances can flocking still occur or are chiral states still possible? If global order is destroyed, could local order in the form of micro-flocks or cliques occur? As a first step to shed light into these problems we consider here a Vicsek-like model with random NRI and tunable alignment bias between the individual particles. This setting includes two different types of scenarios: 1) a group of flocking animals of the same species is comprised of individuals with a common alignment bias but assigns NR corrections to the directional information received from other individuals, corresponding to weak NR randomness, and 2) a multi-species ensemble of self-propelled particles, in which each particle belongs to a different species and has its own NR alignment/anti-alignment rules with each of the other particles, corresponding to strong NR randomness. We will show that both scenarios bear the potential for collective phenomena absent in the conventional one- or two-species flocking models.

*Model:* – We consider  $N$  self-propelled particles or agents  $i$ , characterized by a position  $\mathbf{r}_i(t) \in L^d$  in a  $d$ -dimensional cube of lateral size  $L$  ( $d = 2$  in this paper, p.b.c.) and a movement direction  $\theta_i(t) \in [0, 2\pi]$ . Their mutual tendency to move in the same direction as friendly neighbors (alignment) or to move in the opposite direction as unfriendly neighbors (anti-alignment) is de-

scribed by a (noise-less) Vicsek-like model [5, 46] defined by the equations of motion

$$\dot{\mathbf{r}}_i(t) = v_0 (\cos(\theta_i(t)), \sin(\theta_i(t))) \quad (1)$$

$$\dot{\theta}_i(t) = - \sum_{j \in \mathcal{N}_i} \left( \frac{J_{ij}}{|\mathcal{N}_i|^\alpha} + \frac{J_0}{|\mathcal{N}_i|} \right) \sin(\theta_i(t) - \theta_j(t)) \quad (2)$$

The alignment/anti-alignment interactions consist of an alignment bias  $J_0 \geq 0$  and of a random part  $J_{ij}$  which can be aligning  $J_{ij} > 0$  or anti-aligning  $J_{ij} < 0$ . The  $J_{ij}$  are random variables with  $\overline{J_{ij}} = 0$ ,  $\overline{J_{ij}^2} = J^2$ , and  $\overline{J_{ij}J_{ji}} = \lambda J^2$ , where  $\lambda \in [-1, 1]$  controls degree of non-reciprocity and  $v_0$  is the self-propulsion speed. We set  $J = 1$  and measure  $J_0$  and time  $t$  in units of  $J$ .

$\mathcal{N}_i$  is the "neighborhood of particle  $i$ , comprising all particles  $j$  in a distance smaller than  $R$ , and  $|\mathcal{N}_i|$  is the number of particles in this neighborhood. In the case of infinite range interactions ( $R \rightarrow \infty$ )  $|\mathcal{N}_i| = N$ . The exponent  $\alpha \in \{1/2, 1\}$  denotes different scalings of the interaction strengths:  $\alpha = 1/2$  has to be chosen in order to obtain a non-trivial mean-field limit  $N, R \rightarrow \infty$ ,  $\alpha = 1$  is legitimate for any finite  $N$  and weights bias and randomness similarly. Coherent motion of a flock is indicated by the order parameter  $\vec{m}(t) = 1/N \sum_i (\cos \theta_i(t), \sin \theta_i(t)) = m(t) \cdot (\cos \psi(t), \sin \psi(t))$ , and flocking occurs when  $m(t) \neq 0$ .

*Infinite-range limit:* – For  $R \rightarrow \infty$ , the particle-particle interactions are independent of the particle positions,  $\mathbf{r}_i$ , and the angles  $\theta_i$  evolve according to eq. (2) with  $|\mathcal{N}_i| = N$ . Flocking occurs when  $J_0$  is larger than a critical alignment bias, which for  $\alpha = 1$  decreases with  $N$  as  $J_{0,c}/\sqrt{N}$  (Fig. 1(a)), with  $J_{0,c} = 1.1$ , implying that flocking emerges for any  $J_0 > 0$  in the limit  $N \rightarrow \infty$ . In contrast, for  $\alpha = 1/2$ , eq. (2) reduces in the limit  $N \rightarrow \infty$  to a self-consistent stochastic single particle dynamics or dynamical mean-field theory (DMFT) [25, 26, 33, 35, 47]. For  $\lambda = 0$ , this DMFT is given by

$$\dot{\theta}(t) = (\varphi_y(t) + J_0 m_y(t)) \cos \theta(t) - (\varphi_x(t) + J_0 m_x(t)) \sin \theta(t) \quad (3)$$

where  $\varphi_a(t)$  for  $a = x, y$  is Gaussian colored noise with zero mean and correlations  $\langle \varphi_a(t) \varphi_a(t') \rangle = C_{ab}(t, t')$  which are self-consistently given by the dynamics of  $\theta$  via  $C_{xx}(t, t') = \langle \cos \theta(t) \cos \theta(t') \rangle_\varphi$ ,  $C_{yy}(t, t') = \langle \sin \theta(t) \sin \theta(t') \rangle_\varphi$ , etc. and the magnetization  $(m_x(t), m_y(t)) = (\langle \cos \theta(t) \rangle_\varphi, \langle \sin \theta(t) \rangle_\varphi)$ . By solving eq. (3) numerically [48], we determine for  $\lambda = 0$  the time dependence of the order parameter  $m(t)$  (Fig. 1(b)) and the stationary auto-correlation function  $C(t) = \lim_{t_0 \rightarrow \infty} C(t + t_0, t_0)$  (Fig. 1(b), inset), which approach exponentially fast either zero in the disordered phase or  $m_s > 0$  and  $m_s^2$ , respectively, in the flocking phase. These results also confirm the flocking transition to be at  $J_{0,c} = 1.1$  for  $\lambda = 0$ . The complete  $J_0$ - $\lambda$  phase diagram obtained by numerically integrating (1) and performing finite-size scaling [49] is shown in Fig. 1(c).

In contrast to the purely relaxational behavior of the DMFT ( $N \rightarrow \infty$ ) of uncorrelated randomness ( $\lambda = 0$ ) the

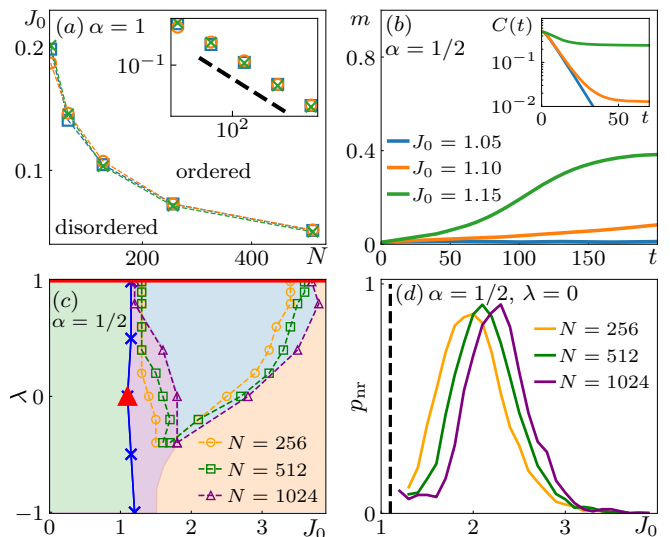


FIG. 1. (a) Infinite range phase diagram for  $\alpha = 1$  and  $\lambda = -0.5$  (circle),  $0$  (square), and  $0.5$  (cross). Inset: Log-log plot of the phase diagram. Black dashed line indicates  $J_0 \sim N^{-1/2}$ . (b) Order parameter  $m(t)$  (3) for different  $J_0$  at  $\lambda = 0$  obtained by solving the DMFT eq.(3). The critical point is  $J_{0,c} \approx 1.1$ . Inset: Correlation function  $C(t)$  for the same values of  $J_0$  as in main figure. (c)  $J_0$ - $\lambda$  phase diagram for  $\alpha = 1/2$ . Green: disordered phase, purple: flocking with relaxational dynamics (c.f. Fig. 2(a)); blue: flocking region with non-relaxational dynamics (c.f. Fig. 2(b-d)), c.f. (d). Note that this region shrinks with increasing  $N$  (see text). Orange: static flocking. The blue line indicates the disorder-flocking phase boundary [49], the red line represents the spin glass region at  $\lambda = 1$ . The red triangle locates the critical point from DMFT at  $\lambda = 0$ . (d) Fraction of disorder-realizations displaying non-relaxational dynamics  $p_{nr}$  as a function of  $J_0$  (at  $\lambda = 0$ ). The black dashed line indicates the critical point from DMFT.  $p_{nr} > 0.15$  defines the blue region in (d).

dynamics of a finite system ( $N < \infty$ ) is much more interesting and can exhibit oscillations, rotations and vibrating oscillations as shown in (Fig. 2(b-d)). These attractors emerge in the whole blue region of Fig. 1(c) within the flocking phase, and persist up to, but not including,  $\lambda = 1$ . At  $\lambda = 1$  eq.(2) predicts a zero-temperature spin glass phase in which the angles  $\theta_i$  relax into a local energy minimum of the underlying XY-Hamiltonian and freeze. We analyze the non-relaxational behavior for finite  $N$  by linearizing the equation of motion by  $\theta_i = \theta_0 + \delta_i$  for  $J_0 \gg J_{0,c}$ . The linearized equation of motion is then

$$\dot{\vec{\delta}} = \mathbf{J}^* \vec{\delta}, \quad (4)$$

where  $[\mathbf{J}^*]_{ij} = J_{ij}/\sqrt{N} + J_0/N$  for  $i \neq j$  and  $[\mathbf{J}^*]_{ii} = -\sum_{j \neq i} [\mathbf{J}^*]_{ij}$ . While the eigenvalue spectrum of the original interaction matrix  $\mathbf{J}$  follows the circular law [50], that of the linearized matrix  $\mathbf{J}^*$  is deformed due to rotational symmetry  $\sum_j [\mathbf{J}^*]_{ij} = 0$  (Fig. 2(e)). The ferromagnetic bias  $J_0$  only shifts the entire eigenvalue spectrum of  $\mathbf{J}^*$  by  $-J_0$  along the  $\text{Re } z$  axis, except for the Goldstone

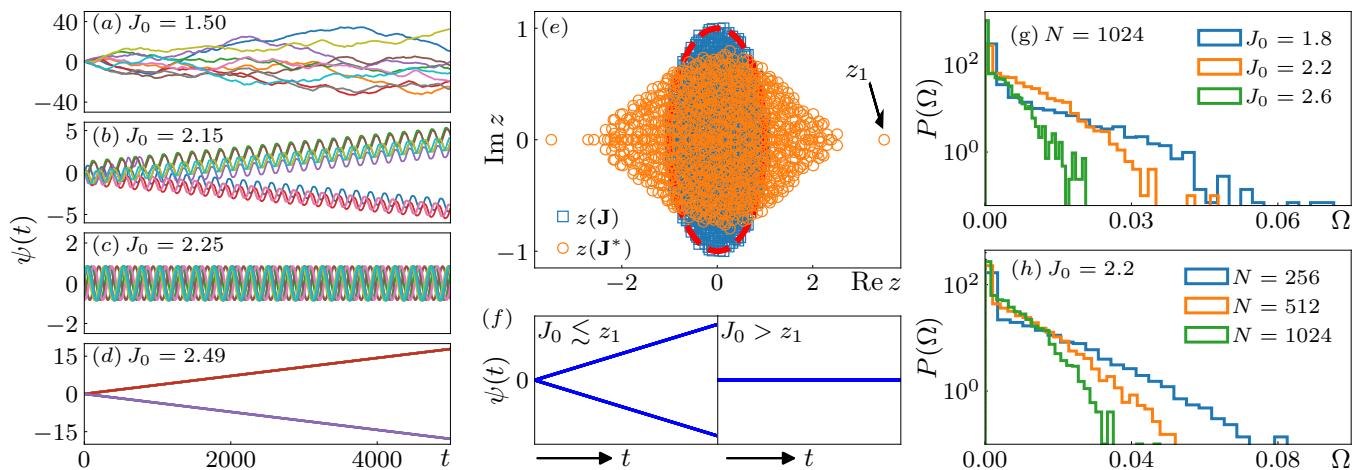


FIG. 2. Emergence of non-relaxational dynamics for finite  $N$  with infinite-range interactions. (a-d) Time evolution of  $\psi(t)$  for a single realization of interaction matrix  $[\mathbf{J}]_{ij} = J_{ij}/\sqrt{N}$  with  $N = 1024$  and  $\lambda = 0$ : (a) flocking with diffusive  $\psi(t)$ , (b) vibrating oscillation, (c) oscillation, and (d) rotation. (e) Eigenvalue spectrum of the same interaction matrix  $\mathbf{J}$  as in (a-d) and the corresponding linearized matrix  $\mathbf{J}^*$ , for  $J_0 = 0$ . The red dashed line indicates the circular law for  $\lambda = 0$  [50] and  $z_1$  depicts the maximum eigenvalue, which locates the critical exceptional point(CEP): Increasing  $J_0$  shifts the spectrum to the left, at the CEP  $z_1 \approx 3.47$  hits zero. (f) Time evolution of  $\psi(t)$  near the CEP.  $J_0 > z_1$  corresponds to the static phase with perfect alignment. For  $J_0 \lesssim z_1$  the system exhibits chiral motion. Clockwise or counter-clockwise rotation depends on the initial condition. (g-h) Probability distribution of the time averaged angular velocity  $P(\Omega)$  in the steady state for fixed  $N$  and varying  $J_0$  in (g) and fixed  $J_0$  and varying  $N$  in (h).

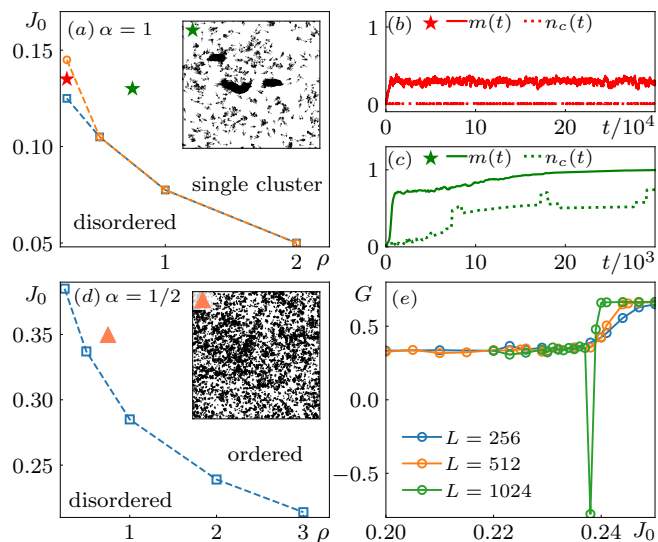


FIG. 3. Finite range interactions ( $R = 1$ ,  $\lambda = 0$ ): (a) Phase diagram for  $\alpha = 1$ . Region between the disordered and the single-cluster phase indicates long range order  $m > 0$  without condensation. Inset: Configuration snapshot ( $L = 1024$ ) of growing clusters in the single cluster region at the point marked with green star in (a). (b,c) Time evolution of magnetization  $m(t)$  and the relative size of the largest cluster  $n_c(t)$  at the red and green point marked in (a). (d) As in (a) for  $\alpha = 1/2$ . Inset: Configuraton snapshot in the ordered region at the orange triangle in (c). (e) Binder cumulant  $G = 1 - \langle m^4 \rangle / (\langle 3m^2 \rangle^2)$  at the transition ( $\rho = 2$ ).

mode  $\mathbf{v}_0 = N^{-1/2}(1, \dots, 1)^T$ , whose eigenvalue remains

at zero.

As  $J_0$  decreases the eigenvector with the eigenvalue  $z = z_1$  coalesces with "the Goldstone mode at  $z = 0$ " [49] at  $J_0 = z_1$ . This is the hallmark of a critical exceptional point (CEP) [52–54] beyond which chiral motion emerges (Fig. 2(f)). At the CEP, all angles still stay close and begin to rotate collectively. As  $J_0$  decreases further, one "outlier"  $\theta_{\text{out}}$  gradually deviates from the the other angles but continues to rotate with them. As soon as the angle-difference reaches  $\pi$ , the chiral motion stops and the static ordered state [49] is restored and remains stable until a second instability arises. The nature of the second instability can be a Hopf bifurcation or again a critical exceptional point, depending on eigenvalue spectrum. In the bulk spectrum, where multiple instabilities contribute, we observe non-relaxational behaviors shown in Fig. 2(b-d) at sufficiently high  $J_0$  (Fig. 1(d)). Notably, the chiral states also exists for finite range interactions if all particles are located within a small circle and have sufficiently small self-propulsion speed  $v_0$  [49].

To render this complex finite- $N$  behavior consistent with the mean-field predictions ( $N \rightarrow \infty$ ) we analyzed the finite-size behavior of the probability distribution of the stationary angular frequency  $\Omega = \langle \psi(t) \rangle$ , where  $\langle \dots \rangle$  denotes a time average. Fig. 2(h) shows that the support of  $P(\Omega)$  shrinks with increasing systems size  $N$ , which implies that any rotational motion of the order parameter becomes on average slower with increasing system size and ceases in the limit  $N \rightarrow \infty$ . We note that even for large but finite system sizes still slow rotations exist, which renders a precise extrapolation of observables to infinite system size by integrating (2) computationally

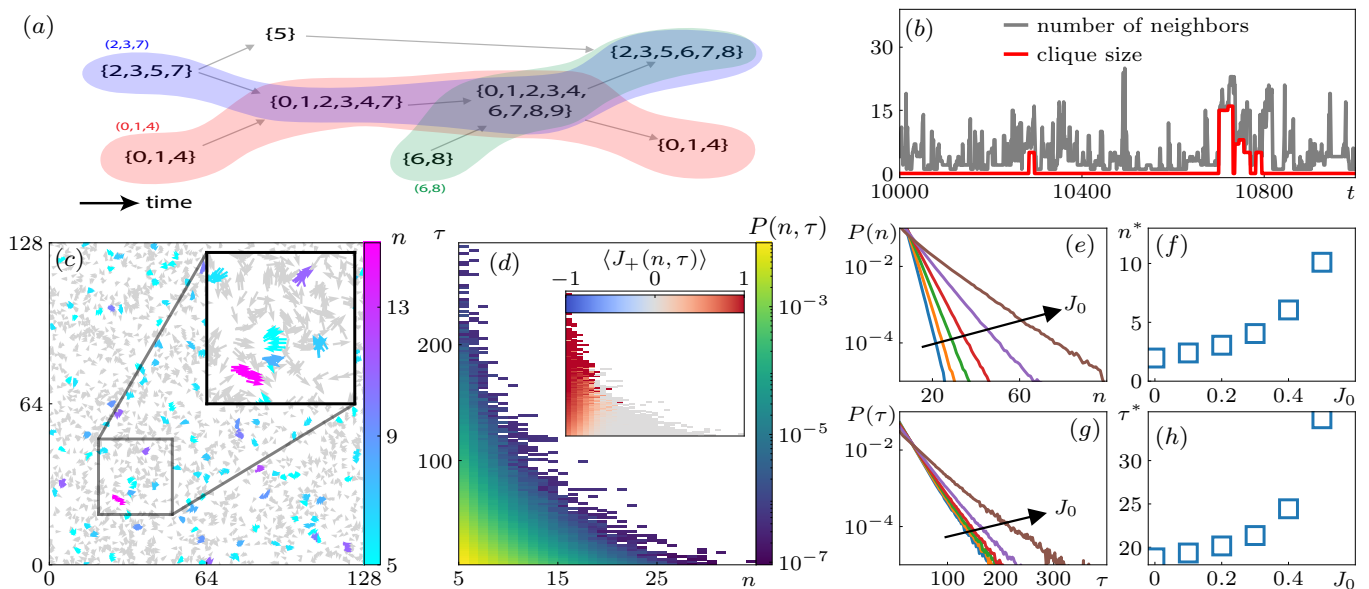


FIG. 4. Clique formation for finite range interactions ( $R = 1$ ,  $\lambda = 0$ ,  $\alpha = 1/2$ ,  $\rho = 0.25$ ). (a) Schematic diagram of the clique detecting algorithm [51]. Each set  $\{\dots\}$  represents connected components and arrow depicts particle flows between connected components in different time. The colored regions indicate three potential cliques:  $\{2, 3, 7\}$  (blue),  $\{0, 1, 4\}$  (red), and  $\{6, 8\}$  (green). (b) Time evolution of the number of interacting neighbors of a specific particle and the size of the largest clique containing it. (c) Snapshot of a particle configuration for  $J_0 = 0$ . Cliques are represented with colors according to its size. Inset: Zoomed-in snapshot of the region indicated by the gray square. (d)  $P(n, \tau)$  at  $J_0 = 0$  averaged over many disorder realization. Inset:  $\langle J_+(n, \tau) \rangle$  at the same parameters as (d). (e-f)  $P(n)$  for different  $J_0$  values and its characteristic cluster size  $n^*$ . (g-h)  $P(\tau)$  for different  $J_0$  values and its characteristic lifetime  $\tau^*$ . The red dashed line in (g,h) represents the critical point  $J_{0,c}$  at  $\rho = 0.25$ .

unfeasible. Nevertheless, the proper  $N \rightarrow \infty$  limit is given by the solution of eq.(3).

*Finite interaction range:* – In the case of a finite interaction range,  $R$ , we integrate (1, 2) using Euler method with time step  $dt = 0.05$ , propulsion speed  $v_0 = 0.5$ . We set  $R = 1$  and discuss here only uncorrelated randomness  $\lambda = 0$ . For  $\alpha = 1$  flocking already occurs for small alignment bias  $J_0 \ll J(= 1)$ , which decreases with increasing density,  $\rho = N/L^2$ , as shown in Fig. 3(a), reminiscent of the decrease of  $J_{0,c}(N)$  with  $N$  for the infinite range case. In the flocking phase, except for small  $\rho$ , the system eventually evolves into a single dense cluster in which all particles are tightly packed and move coherently (inset of Fig. 3(a)). This single-cluster phase emerges via nucleation: once a denser cluster forms, the contribution of the alignment bias to the interactions dominates over the random contribution due to the  $\alpha = 1$  scaling, such that the cluster eventually absorbs all particles (Fig. 3(c)).

For  $\alpha = 1/2$ , the critical alignment bias,  $J_{0,c}$ , also decreases with increasing density,  $\rho$ , as shown in (Fig. 3(d)). Here the flocking phase does not consist of a single cluster as for  $\alpha = 1$ , but is a globally ordered state since the  $\alpha = 1/2$  scaling does not suppress the randomness at large local densities. The transition from the disordered phase to the flocking phase is discontinuous (Fig. 3(e)), reminiscent of the Vicsek model [46, 55]. In contrast to the Vicsek model, the system does not exhibit a coexistence phase, and the density profile remains homoge-

neous (Fig. 3(d)).

*Clique formation:* – Instead, both disordered and ordered phase in the low density regime are characterized by clique formation, where transient clusters of coherently moving particles emerge and disintegrate dynamically even in absence of a ferromagnetic bias  $J_0 = 0$ . To analyze these cliques, we construct interaction networks based on distance between particles at successive simulation times and track the evolution of their connected components [51] (Fig. 4(a)). Among the connected components that persist over time, we define a ‘clique’  $\mathcal{C}(n, \tau)$  as a set of particles in a connected component with size  $n$  and lifetime  $\tau$ , restricted to those with  $n \geq 5$  and  $\tau \geq 10$  (Fig. 4(c)). Fig. 4(b) represents an example time series for a specific particle, illustrating that only a small subset of its interacting neighbors actually form cliques with it. Fig. 4(d) shows  $P(n, \tau)$ , the probability that a particle belongs to  $\mathcal{C}(n, \tau)$ , averaged over time and disorder. Both  $P(n)$  and  $P(\tau)$  exhibit exponential tail (Fig. 4(e),(g)) and the characteristic clique size  $n^*$  and lifetime  $\tau^*$  are extracted from exponential fits (Fig. 4(f),(h)). Notably, here the life-time  $\tau$  of medium- and small-size cliques is actually sufficiently long for them to traverse half of the system.

The formation of a clique is driven by the self-assembly of particles with predominantly mutual aligning interactions  $\langle J_+(n, \tau) \rangle > 0$ , where  $J_+(n, \tau)$  is an average of  $J_{ij} + J_{ji}$  over the members  $i, j$  of a clique, as shown in the

inset of Fig. 4(d). Cliques disintegrate when they collide with other strongly interacting particles or cliques [49]. When compared with clusters emerging in the disordered phase of the conventional Vicsek model with homogeneous alignment interactions one notes that in the latter clusters are typically larger but have shorter life-times.

*Conclusion* – We have shown that flocking can occur in an ensemble of self-propelled particles with a random mixture of non-reciprocal aligning and ant-aligning interactions. It turns out that the scaling of the interactions with the number of interaction neighbors is crucial: if the alignment bias and the random part scale identical, flocking always emerges at sufficiently large density. If they scale differently such to produce a non-trivial mean-field limit, long-range order only exists for sufficiently large alignment bias and additional complex states emerge: spurious chiral states for finite systems and intermittent self-assembled cliques even without alignment bias. In a subsequent publication [56] we discuss the robustness of

these phenomena in the presence of noise or the introduction of the Vicsek update rules for directional changes. Also the variation of the degree of non-reciprocity bears interesting aspects as an enhanced tendency to order for  $\lambda \rightarrow 1$  and an emerging spin glass phase at  $\lambda = 1$ .

Our results may serve as a starting point for the study of multi-species flocking models with non-random but complex non-reciprocal inter-species interactions in the following sense: As non-reciprocal interactions are used to generate temporal sequences of patterns in neural network models [24] or for dynamical control of self-assembled immobile structures and transitions between [57] we expect that programmable non-reciprocal interactions in flocking models as the one analyzed here could be a tool to create mobile "shape-shifters" made of self-propelled particles that arrange in a pre-determined temporal sequence of patterns with varying shapes. It would be worthwhile to examine this vision in future work.

- 
- [1] M. C. Marchetti, J. F. Joanny, S. Ramaswamy, T. B. Liverpool, J. Prost, M. Rao, and R. A. Simha, Hydrodynamics of soft active matter, *Rev. Mod. Phys.* **85**, 1143 (2013).
  - [2] S. Ramaswamy, The mechanics and statistics of active matter, *Annual Review of Condensed Matter Physics* **1**, 323 (2010).
  - [3] C. Bechinger, R. Di Leonardo, H. Löwen, C. Reichhardt, G. Volpe, and G. Volpe, Active particles in complex and crowded environments, *Rev. Mod. Phys.* **88**, 045006 (2016).
  - [4] M. R. Shaebani, A. Wysocki, R. G. Winkler, G. Gompper, and H. Rieger, Computational models for active matter, *Nature Reviews Physics* **2**, 181 (2020).
  - [5] T. Vicsek, A. Czirók, E. Ben-Jacob, I. Cohen, and O. Shochet, Novel type of phase transition in a system of self-driven particles, *Phys. Rev. Lett.* **75**, 1226 (1995).
  - [6] M. E. Cates and J. Tailleur, Motility-induced phase separation, *Annual Review of Condensed Matter Physics* **6**, 219 (2015).
  - [7] A. Bricard, J.-B. Caussin, N. Desreumaux, O. Dauchot, and D. Bartolo, Emergence of macroscopic directed motion in populations of motile colloids, *Nature* **503**, 95–98 (2013).
  - [8] V. Schaller, C. Weber, C. Semmrich, E. Frey, and A. R. Bausch, Polar patterns of driven filaments, *Nature* **467**, 73–77 (2010).
  - [9] I. Theurkauff, C. Cottin-Bizonne, J. Palacci, C. Ybert, and L. Bocquet, Dynamic clustering in active colloidal suspensions with chemical signaling, *Phys. Rev. Lett.* **108**, 268303 (2012).
  - [10] J. Palacci, S. Sacanna, A. P. Steinberg, D. J. Pine, and P. M. Chaikin, Living crystals of light-activated colloidal surfers, *Science* **339**, 936–940 (2013).
  - [11] F. A. Lavergne, H. Wendehenne, T. Bäuerle, and C. Bechinger, Group formation and cohesion of active particles with visual perception-dependent motility, *Science* **364**, 70–74 (2019).
  - [12] L. Barberis and F. Peruani, Large-scale patterns in a minimal cognitive flocking model: Incidental leaders, nematic patterns, and aggregates, *Physical Review Letters* **117**, 10.1103/physrevlett.117.248001 (2016).
  - [13] M. Fruchart, R. Hanai, P. B. Littlewood, and V. Vitelli, Non-reciprocal phase transitions, *Nature* **592**, 363–369 (2021).
  - [14] K. L. Kreienkamp and S. H. L. Klapp, Nonreciprocal alignment induces asymmetric clustering in active mixtures, *Phys. Rev. Lett.* **133**, 258303 (2024).
  - [15] M. Mangeat, S. Chatterjee, J. D. Noh, and H. Rieger, Emergent complex phases in a discrete flocking model with reciprocal and non-reciprocal interactions, *Communications Physics* **8**, 186 (2025).
  - [16] Y. Avni, M. Fruchart, D. Martin, D. Seara, and V. Vitelli, Nonreciprocal Ising model, *Phys. Rev. Lett.* **134**, 117103 (2025).
  - [17] Y. Avni, M. Fruchart, D. Martin, D. Seara, and V. Vitelli, Dynamical phase transitions in the nonreciprocal Ising model, *Phys. Rev. E* **111**, 034124 (2025).
  - [18] Z. You, A. Baskaran, and M. C. Marchetti, Nonreciprocity as a generic route to traveling states, *Proceedings of the National Academy of Sciences* **117**, 19767–19772 (2020).
  - [19] F. Brauns and M. C. Marchetti, Nonreciprocal pattern formation of conserved fields, *Phys. Rev. X* **14**, 021014 (2024).
  - [20] D. Banerjee, A. Souslov, A. G. Abanov, and V. Vitelli, Odd viscosity in chiral active fluids, *Nature Communications* **8**, 1573 (2017).
  - [21] C. Scheibner, A. Souslov, D. Banerjee, P. Surówka, W. T. M. Irvine, and V. Vitelli, Odd elasticity, *Nature Physics* **16**, 475 (2020).
  - [22] C. Hargus, J. M. Epstein, and K. K. Mandadapu, Odd diffusivity of chiral random motion, *Phys. Rev. Lett.* **127**, 178001 (2021).
  - [23] E. Kalz, H. D. Vuijk, I. Abdoli, J.-U. Sommer, H. Löwen, and A. Sharma, Collisions enhance self-diffusion in odd-

- diffusive systems, *Phys. Rev. Lett.* **129**, 090601 (2022).
- [24] H. Sompolinsky and I. Kanter, Temporal association in asymmetric neural networks, *Physical Review Letters* **57**, 2861–2864 (1986).
- [25] A. Crisanti and H. Sompolinsky, Dynamics of spin systems with randomly asymmetric bonds: Langevin dynamics and a spherical model, *Physical Review A* **36**, 4922–4939 (1987).
- [26] H. Rieger, M. Schreckenberg, and J. Zittartz, Glauber dynamics of neural network models, *Journal of Physics A: Mathematical and General* **21**, L263 (1988).
- [27] H. Sompolinsky, A. Crisanti, and H. J. Sommers, Chaos in random neural networks, *Phys. Rev. Lett.* **61**, 259 (1988).
- [28] H. Rieger, Solvable model of a complex ecosystem with randomly interacting species, *Journal of Physics A: Mathematical and General* **22**, 3447–3460 (1989).
- [29] A. Altieri, F. Roy, C. Cammarota, and G. Biroli, Properties of equilibria and glassy phases of the random lotka-volterra model with demographic noise, *Phys. Rev. Lett.* **126**, 258301 (2021).
- [30] V. Ros, F. Roy, G. Biroli, G. Bunin, and A. M. Turner, Generalized lotka-volterra equations with random, non-reciprocal interactions: The typical number of equilibria, *Phys. Rev. Lett.* **130**, 257401 (2023).
- [31] G. Garcia Lorenzana, A. Altieri, and G. Biroli, Interactions and migration rescuing ecological diversity, *Phys. Rev. X Life* **2**, 013014 (2024).
- [32] G. Parisi, A simple model for the immune network., *Proceedings of the National Academy of Sciences* **87**, 429–433 (1990).
- [33] J. C. Stiller and G. Radons, Dynamics of nonlinear oscillators with random interactions, *Physical Review E* **58**, 1789–1799 (1998).
- [34] A. Prüser, S. Rosmej, and A. Engel, Nature of the volcano transition in the fully disordered kuramoto model, *Phys. Rev. Lett.* **132**, 187201 (2024).
- [35] A. Prüser and A. Engel, Role of coupling asymmetry in the fully disordered kuramoto model, *Phys. Rev. E* **110**, 064214 (2024).
- [36] R. Hanai, Nonreciprocal frustration: Time crystalline order-by-disorder phenomenon and a spin-glass-like state, *Phys. Rev. X* **14**, 011029 (2024).
- [37] L. Parkavousi, N. Rana, R. Golestanian, and S. Saha, Enhanced stability and chaotic condensates in multispecies nonreciprocal mixtures, *Phys. Rev. Lett.* **134**, 148301 (2025).
- [38] Y. Duan, B. Mahault, Y.-q. Ma, X.-q. Shi, and H. Chaté, Breakdown of ergodicity and self-averaging in polar flocks with quenched disorder, *Phys. Rev. Lett.* **126**, 178001 (2021).
- [39] O. Chepizhko, E. G. Altmann, and F. Peruani, Optimal noise maximizes collective motion in heterogeneous media, *Phys. Rev. Lett.* **110**, 238101 (2013).
- [40] A. Chardac, S. Shankar, M. C. Marchetti, and D. Bartolo, Emergence of dynamic vortex glasses in disordered polar active fluids, *Proceedings of the National Academy of Sciences* **118**, e2018218118 (2021).
- [41] A. Morin, N. Desreumaux, J.-B. Caussin, and D. Bartolo, Distortion and destruction of colloidal flocks in disordered environments, *Nature Physics* **13**, 63–67 (2016).
- [42] J. Codina, B. Mahault, H. Chaté, J. Dobnikar, I. Pagonabarraga, and X.-q. Shi, Small obstacle in a large polar flock, *Physical Review Letters* **128**, 10.1103/physrevlett.128.218001 (2022).
- [43] S. Ro, Y. Kafri, M. Kardar, and J. Tailleur, Disorder-induced long-ranged correlations in scalar active matter, *Phys. Rev. Lett.* **126**, 048003 (2021).
- [44] Y. Ben Dor, S. Ro, Y. Kafri, M. Kardar, and J. Tailleur, Disordered boundaries destroy bulk phase separation in scalar active matter, *Phys. Rev. E* **105**, 044603 (2022).
- [45] S. Chatterjee, M. Mangeat, C.-U. Woo, H. Rieger, and J. D. Noh, Flocking of two unfriendly species: The two-species vicsek model, *Phys. Rev. E* **107**, 024607 (2023).
- [46] G. Grégoire and H. Chaté, Onset of collective and cohesive motion, *Phys. Rev. Lett.* **92**, 025702 (2004).
- [47] G. G. Lorenzana, A. Altieri, G. Biroli, M. Fruchart, and V. Vitelli, Non-reciprocal spin-glass transition and aging (2024), arXiv:2408.17360 [cond-mat.dis-nn].
- [48] F. Roy, G. Biroli, G. Bunin, and C. Cammarota, Numerical implementation of dynamical mean field theory for disordered systems: application to the lotka-volterra model of ecosystems, *Journal of Physics A: Mathematical and Theoretical* **52**, 484001 (2019).
- [49] See Supplemental Material at URL-will-be-inserted-by-publisher.
- [50] H. J. Sommers, A. Crisanti, H. Sompolinsky, and Y. Stein, Spectrum of large random asymmetric matrices, *Phys. Rev. Lett.* **60**, 1895 (1988).
- [51] K. Buchin, M. Buchin, M. v. Kreveld, B. Speckmann, and F. Staals, Trajectory grouping structure, *Journal of Computational Geometry* **6**, 75–98 (2015).
- [52] R. Hanai and P. B. Littlewood, Critical fluctuations at a many-body exceptional point, *Phys. Rev. Res.* **2**, 033018 (2020).
- [53] C. P. Zelle, R. Daviet, A. Rosch, and S. Diehl, Universal phenomenology at critical exceptional points of nonequilibrium  $O(n)$  models, *Phys. Rev. X* **14**, 021052 (2024).
- [54] T. Suchanek, K. Kroy, and S. A. M. Loos, Time-reversal and parity-time symmetry breaking in non-hermitian field theories, *Phys. Rev. E* **108**, 064123 (2023).
- [55] H. Chaté, F. Ginelli, G. Grégoire, and F. Raynaud, Collective motion of self-propelled particles interacting without cohesion, *Phys. Rev. E* **77**, 046113 (2008).
- [56] J. Choi, H. Rieger, to be published (2025).
- [57] S. Osat and R. Golestanian, Non-reciprocal multifarious self-organization, *Nature Nanotechnology* **18**, 79–85 (2022).

## Supplemental material: Flocking with random non-reciprocal interactions

Jiwon Choi<sup>1</sup>, Jae Dong Noh<sup>2</sup>, Heiko Rieger<sup>1</sup>

<sup>1</sup> *Department of Physics & Center for Biophysics,  
Saarland University, Campus E2 6, 66123 Saarbrücken, Germany*  
<sup>2</sup> *Department of Physics, University of Seoul, Seoul, 02504, Korea*

### I. FINITE SIZE SCALING AT THE CRITICAL POINT $J_{0,c}$

In the infinite range limit we determine  $N$ -dependent critical point  $J_{0,c}(N)$  For  $\alpha = 1$  using the order parameter susceptibility, defined as

$$\chi(J_0, N) = N (\langle m^2 \rangle - \langle m \rangle^2) \quad (S1)$$

where  $\langle \dots \rangle$  denotes an average over time and over the random matrices  $J_{ij}$ , and the order parameter is given by  $m(t)e^{i\psi(t)} = N^{-1} \sum_j e^{i\theta_j(t)}$ . We define  $J_{0,c}(N)$  as the values of  $J_0$  at which the order parameter susceptibility reaches its maximum (Fig.S1(a)).

In the infinite-range limit, the cases  $\alpha = 1$  and  $\alpha = 1/2$  differ only by the scaling of nonreciprocal alignment. Therefore, for any finite  $N$  the properties of the system with  $\alpha = 1/2$  at alignment bias  $J_0$  are equivalent to the properties of the system with  $\alpha = 1$  at alignment bias  $J_0\sqrt{N}$ . We confirm this relation by computing the Binder cumulant, defined as

$$G = 1 - \frac{\langle m^4 \rangle}{3\langle m^2 \rangle^2} \quad (S2)$$

The critical point of the infinite system ( $N \rightarrow \infty$ ,  $\alpha = 1/2$ ) is given by the intersection point of the Binder cumulant  $G$  for different  $N$ . For both cases, for  $\alpha = 1$  (after rescaling of  $J_0$ ) and  $\alpha = 1/2$ , the intersection point is at  $J_{0,c} \approx 1.1$ , which is consistent with the mean field prediction from eq.(3) of the main text.

For general  $\lambda \neq 0$  the disorder-flocking transition line in Fig.1(c) in the main text is also obtained by using finite size scaling and the Binder cumulant.

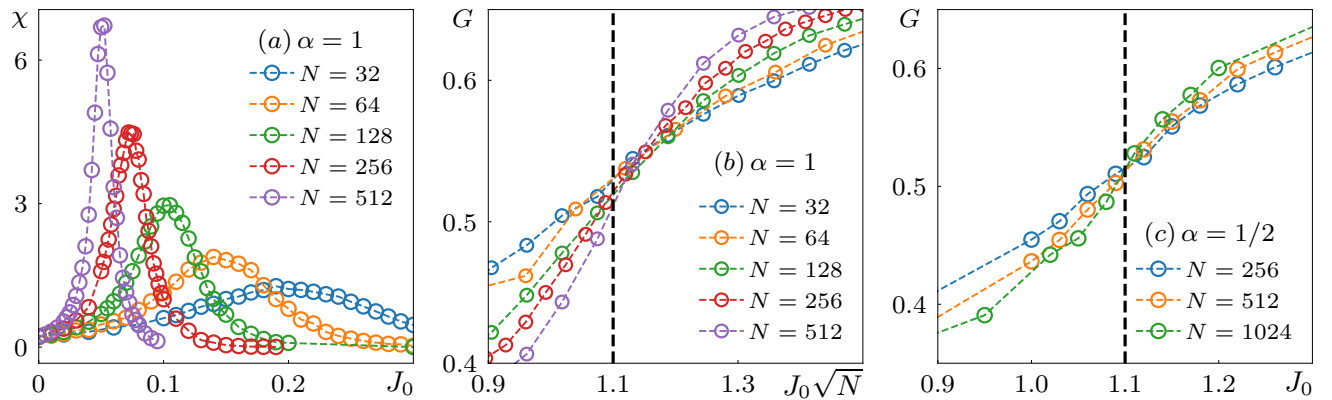


FIG. S1. (a) Order parameter susceptibility  $\chi$  for the  $\alpha = 1$  case. (b-c) Binder cumulant  $G$  across the flocking transition for (b)  $\alpha = 1$  with rescaled  $J_0$ , and (c)  $\alpha = 1/2$ . The black dashed line indicates the critical point obtained from DMFT.

### II. CHIRAL STATES IN FINITE SYSTEMS (INFINITE RANGE, $\lambda = 0$ )

In this section, we show that the rotational motion at  $J_0 = z_1$  originates from the critical exceptional point (CEP). We mainly focus on a single realization of interaction matrix, shown in Fig. 2(d) in the main text, but the qualitative behaviors remain robust for other realizations.

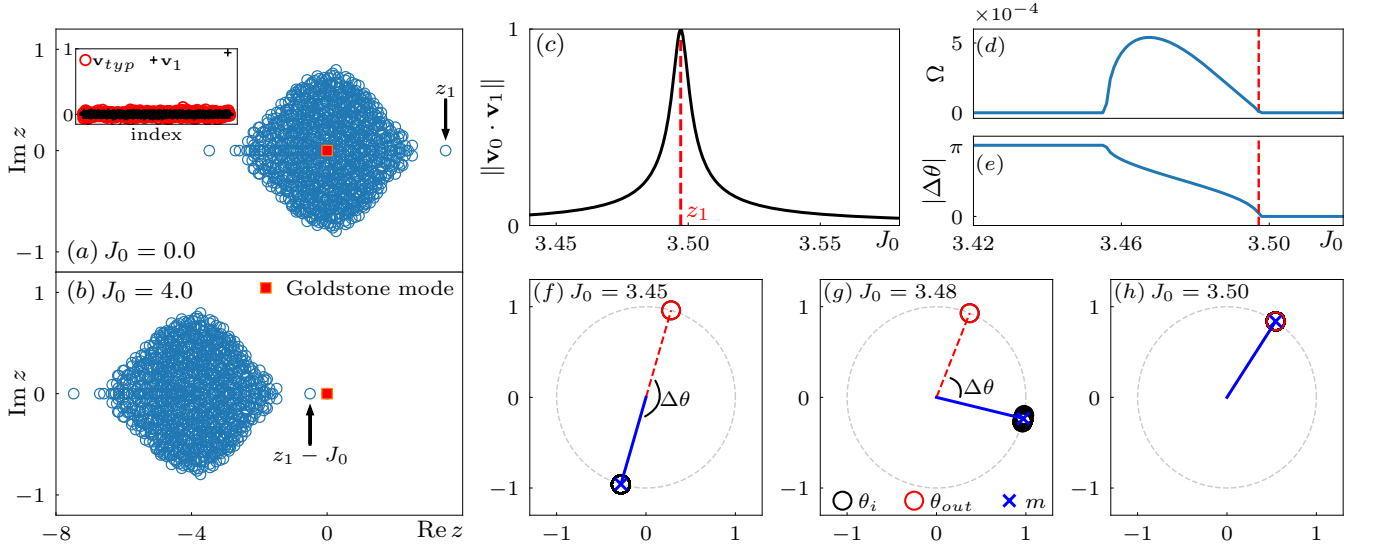


FIG. S2. Eigenvalue spectrum of  $\mathbf{J}^*$  with (a)  $J_0 = 0$  and (b)  $J_0 = 4.0$ . The red square depicts the Goldstone mode  $\mathbf{v}_0 = N^{-1/2}(1, \dots, 1)$  and  $z_1$  denotes the largest eigenvalue of  $\mathbf{J}^*$ . Inset in (a): Components of a typical bulk eigenvector  $\mathbf{v}_{\text{typ}}$  (red circles) and the leading eigenvector  $\mathbf{v}_1$  associated with  $z_1$  at  $J_0 = 0$  (black pluses).  $\mathbf{v}_1$  exhibits highly localized structure, and we refer to its largest component as the 'outlier component'. This outlier component is depicted as a red circle in (f-h), where it drives global chiral motion. (c) Overlap between the leading eigenvector  $\mathbf{v}_1$  and the Goldstone mode  $\mathbf{v}_0$ . The peak at  $J_0 = z_1$  indicates their coalescence. (d) Steady-state angular frequency  $\Omega \equiv \langle \dot{\psi}(t) \rangle$ . (e) Angle difference between the outlier component and the order parameter  $\Delta\theta \equiv \theta_{\text{out}} - \psi$ . (f-h) Steady-state configurations  $\{\theta_i\}$  at different  $J_0$  values: (f)  $J_0 = 3.45$ , (g)  $J_0 = 3.48$ , and (h)  $J_0 = 3.50$ . See also 'movie1'. The red circle depicts the outlier component  $\theta_{\text{out}}(t)$ , corresponding to maximum component of  $\mathbf{v}_1$  (see inset of (a)).

In mean-field limit with  $\alpha = 1/2$ , the equation of motion reduces to

$$\dot{\theta}_i(t) = - \sum_j \left( \frac{J_{ij}}{\sqrt{N}} + \frac{J_0}{N} \right) \sin(\theta_i(t) - \theta_j(t)) \quad (\text{S3})$$

When  $J_0 \gg 1.1J$ , phase differences between oscillators become negligible, thus the system remains perfectly synchronized state  $\theta_i(t) = \psi(t) + \delta_i(t)$ , where  $\psi(t)$  denotes the phase of magnetization. In this limit, we can approximate (S3) as

$$\dot{\delta}_i = - \sum_j \left( \frac{J_{ij}}{\sqrt{N}} + \frac{J_0}{N} \right) (\delta_i - \delta_j) \quad \Rightarrow \quad \dot{\vec{\delta}} = \mathbf{J}^* \vec{\delta} \quad (\text{S4})$$

where the components of linearized interaction matrix  $\mathbf{J}^*$  are given by  $[\mathbf{J}^*]_{ij} = J_{ij}/\sqrt{N} + J_0/N$  for  $i \neq j$  and  $[\mathbf{J}^*]_{ii} = \sum_{j \neq i} [\mathbf{J}^*]_{ij}$ . The diagonal component forces the zero-row-sum condition  $\sum_j [\mathbf{J}^*]_{ij} = 0$ , which originates from the rotational invariance of (S3). As a consequence, the Goldstone mode  $\mathbf{v}_0 = N^{-1/2}(1, \dots, 1)$  associated with rotational invariance exists with zero eigenvalue  $z_0 = 0$ , marked in Fig. S1(a,b).

Although the eigenvalue spectrum of the interaction matrix  $[\mathbf{J}]_{ij} = J_{ij}/\sqrt{N}$  exhibits the circular law [50], rotational invariance significantly deforms the eigenvalue spectrum. In addition, the presence of ferromagnetic bias  $J_0$  acts as a rank-1 perturbation on  $\mathbf{J}^*$ , which uniformly shifts the whole spectrum by  $-J_0$  along the  $\text{Re } z$  axis, except for the Goldstone mode (Fig. S2(a,b)). As a result, when  $J_0 > z_1$ , where  $z_1$  denotes the largest eigenvalue, all eigenvalues have a negative real part and only the Goldstone mode remains at  $z = 0$ . As  $J_0 (> z_1)$  decreases,  $z_1$  approaches  $z = 0$  and eventually collides with the Goldstone mode at  $J_0 = z_1$ . And the eigenvector  $\mathbf{v}_1$  associated with  $z_1$  coalesces with the Goldstone mode  $\mathbf{v}_0$  at this point, indicating the CEP (Fig. S2(c)) [52–54].

As soon as  $J_0$  crosses the CEP, the system exhibits spontaneous chiral motion, where all oscillators rotate with a constant angular velocity  $\Omega$ , see Fig. S2(c) and 'movie1'. The direction of chiral motion depends on the initial condition, and we generally observe counter-clockwise and clockwise rotation with an equal probability. When the chiral motion takes a place, the steady-state configuration  $\{\theta_i\}$  has a special structure: While all other oscillators remain close each other, an 'outlier'  $\theta_{\text{out}}$  maintains non-zero angle difference with them, which is described by  $\Delta\theta =$

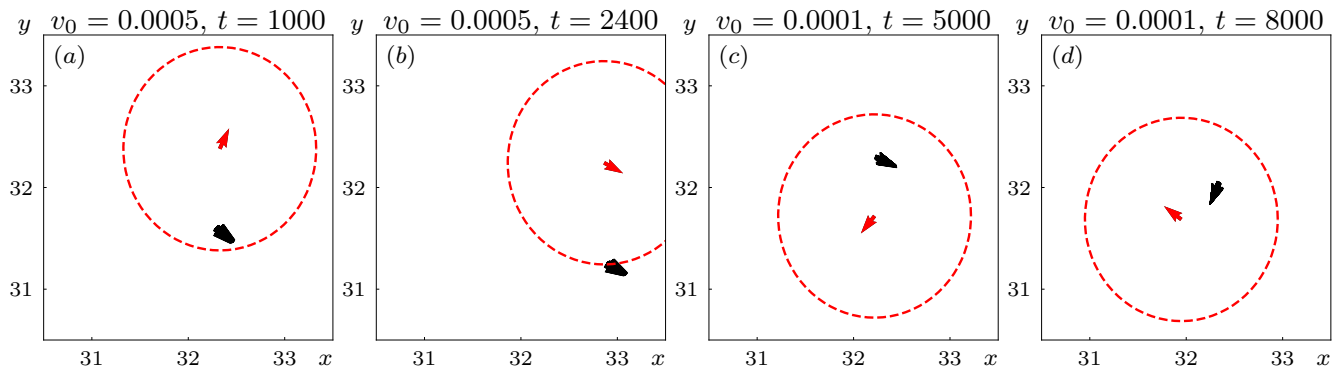


FIG. S3. Snapshots from ‘movie3’ for different self-propulsion speeds: (a,b)  $v_0 = 0.0005$  and (c,d)  $v_0 = 0.0001$ . The red arrow and circle depict  $\theta_{\text{out}}$  and its interaction range. For larger  $v_0$ (a,b),  $\theta_{\text{out}}$  partially loses its interacting neighbors as it moves, and whole system restores perfect alignment. In contrast, for small  $v_0$ (c,d), all particles remains within their interaction range and chiral motion is stable.

$\theta_{\text{out}} - \psi$ (Fig. S2(f-h)). The angle difference increases as  $J_0$  decreases(Fig.S2(e)) and reaches  $\pi$ . The steady-state angular frequency approaches to zero as  $\Delta\theta$  approaches  $\pi$ (Fig.S2(e)), and static flocking phase is restored where only ‘outlier’ points opposite direction with others(Fig.S2(f)).

The second instability appears as the second largest eigenvalue hits zero. Its nature depends on disorder realization: When second largest eigenvalue is real(or complex with its conjugate), then it exhibits CEP(oscillatory instability). Observed complex behaviors in the main text appear in bulk spectrum region, where multiple instabilities contribute.

### III. CHIRAL STATES WITH FINITE INTERACTION RANGE

In this section, we discuss the possibility of spontaneous chiral motion with a finite interaction range. As in the main text, we set the interaction range to  $R = 1$ . We find that a spontaneous chiral state can emerge in finite interaction range, but only under specific initial conditions: All particles are located in a small region(smaller than  $R$ ) and the propulsion speed  $v_0$  should be sufficiently small. The initial orientations can be randomly assigned.

Fig. S3(see also ‘movie3’) shows such a case at  $J_0 = 3.47$  using the same interaction matrix as Fig. S2 for different  $v_0$ . Starting from the given initial conditions, the system gradually develops a spontaneous chiral motion with the same angular frequency  $\Omega$ , provided that all inter-particle distances stay within the interaction range  $R$ . Since each particle follows a circular motion of radius  $r = v_0/\Omega$ , the condition that this chiral state remains stable is given by  $v_0 \lesssim \Omega$ . If  $v_0$  exceeds the threshold,  $\theta_{\text{out}}$  loses some interaction neighbors(Fig. S3(a,b)), and the coherent chiral motion breaks down. In contrast, for the case where  $v_0$  is sufficiently small, the chiral motion remains stable(Fig. S3(c,d)).

### IV. DESCRIPTION OF SUPPLEMENTAL MOVIES

The interaction matrix used in movies (1-3) is identical to that in Fig. 2 of the main text. Movies are also available at <https://doi.org/10.5281/zenodo.15742180>.

- movie 1: Emergence of spontaneous chiral motion near the critical exceptional point(CEP). Parameters:  $N = 1024$  and  $\lambda = 0$ .
- movie 2: Various phase behaviors in flocking phase: (a) flocking with relaxational dynamics, (b) vibrating oscillation, (c) oscillation, and (d) rotation. Parameters:  $N = 1024$  and  $\lambda = 0$ .
- movie 3: Chiral state in finite-range interactions. The system starts from an initial condition where particles are confined within a small region and have random initial orientations. Parameters:  $N = 1024$ ,  $\lambda = 0$ , and  $J_0 = 3.47$ .
- movie 4: Clique formation in steady-state at  $J_0 = 0$ . The color represents the size of each clique, and black arrows indicates long-living pair(or triplet) with lifetime  $\tau > 150$ . Parameters:  $L_x = L_y = 128$ ,  $\lambda = 0$ ,  $\rho = 0.25$ ,  $R = 1$ , and  $J_0 = 0$ .